RESEARCH ARTICLE

WILEY **Journal of RAMAN SPECTROSCOPY**

SERS spectrum of imazalil. Experimental and quantum-chemical vibrational analysis

Gonzalo Díaz-Mirón[1] | María A. Sánchez[2,3] | Doly M. Chemes[1] | Rosa M.S. Álvarez[1,4] (iD)

[1] Instituto de Química Física–Facultad de Bioquímica, Química y Farmacia, Universidad Nacional de Tucumán, San Lorenzo 456, 4000 Tucumán, Argentina

[2] Laboratorio de Medios e Interfases, Departamento de Bioingeniería, Facultad de Ciencias Exactas y Tecnología, Universidad Nacional de Tucumán, Av. Independencia 1800, 4000 Tucumán, Argentina

[3] Instituto Superior de Investigaciones Biológicas (INSIBIO), CONICET, Tucumán, Argentina

[4] Instituto de Química del Noroeste Argentino (INQUINOA), CONICET, Tucumán, Argentina

Correspondence
Rosa M. S. Álvarez, Instituto de Química Física–Facultad de Bioquímica, Química y Farmacia, Universidad Nacional de Tucumán, San Lorenzo 456, 4000 Tucumán, Argentina.
Email: myshukoalvarez@gmail.com; mysuko@fbqf.unt.edu.ar

Abstract

Imazalil [1-[2-(2,4-dichlorophenyl)-2-(2-propenyloxyl-ethyl]-1 H imidazole] is a systemic fungicide that is toxic to a number of plant pathogens, particularly species of Penicillum. Its activity is based on the inhibition of mold sporulation on fruit skin, which makes it one of the most commonly used fungicide in post-harvest citrus treatments for fruit preservation during storage, shipping, and marketing. Due to its wide application, the presence of imazalil needs to be monitored to avoid the excessive and/or improper use. This work reports a complete analysis of the Fourier-transform infrared spectroscopy and Raman spectra of imazalil as a pure compound as well as in the commercial product for agricultural use; the band assignment relays in the vibrational predictions acquired by quantum-chemical calculations (B3LYP/6–311 + g(2df, p)) for the imazalil molecule. An analytical application of surface-enhanced Raman spectroscopy (SERS) is also presented here. It is done so by using a novel, low-cost, and sensitive SERS-active substrate built with silver nanoparticles supported on a Si/ZnO nanowires platform to detect traces of imazalil in aqueous solutions. Comparison between the Raman and SERS spectra allowed the characterization of the interaction between the pesticide and the silver nanoparticle surface.

KEYWORDS
imazalil, pesticide, Raman, SERS

1 | INTRODUCTION

Several types of pesticide are commonly used in agriculture in order to protect crops and seeds against mold, blight, and other diseases that may appear during transportation and long-time deposit. This practice must be performed under strict control to ensure food safety, because the residues of pesticides remain in fruits causing environmental impact and public health risks. Although pesticides are designed to offer high specificity of action, their use is also manifested in innumerable undesirable effects as the appearance of resistant organisms and the contamination of water and soil with carcinogenic, mutagenic, or toxic substances.[1]

Current standard methods applied to control and monitor the excessive and/or improper use of pesticides and herbicides are based on HPLC and CG-MS techniques,[2–5] which are known to be time consuming and require expensive experimental approach and sophisticated laboratories. Surface-enhanced Raman spectroscopy (SERS) is a label-free detection method able to provide high sensitivity, offering remarkable potential for analytical applications in fast and simple protocols and relatively cheap experiments. These properties have lead SERS to

emerge in the last decades as a valuable alternative to detect contaminants in the food that reaches the consumer's table.[6–11] The enhancement of the Raman scattering intensity of molecules at the trace level is propitiated by the presence of a nanostructured metallic surface[12] and is associated with localized surface plasmon resonance induced on the metal surface.[13] This fact has made the development of SERS substrates a very active field in the pursuit of efficiency, sensibility, and ease of use.[14]

Imazalil [1-[2-(2,4-dichlorophenyl)-2-(2-propenyloxyl-ethyl]-1 H imidazole] is one of the most commonly used fungicide in citrus postharvest treatments for the preservation of fruits during storage, shipment, and marketing, because it inhibits the sporulation of mold on the fruit skin.[15] Imazalil is a systemic fungicide that is toxic to a number of plant pathogens, particularly species of Penicillum, by acting as an inhibitor of the ergosterol biosynthesis.[16]

In spite of the wide application of imazalil and the consequent need for its control and monitoring, the vibrational analysis of this substance has not yet been published. In this work, we report the first complete study of the infrared and Raman spectra of the imazalil; the experimental data were complemented by quantum chemical calculations (B3LYP/6–311 + g(2df,p)) that provided the basis for the interpretation of the vibrational behavior of this molecule. The vibrational spectra of the agricultural commercial formula were also collected and compared with those of the pure imazalil. Because the inspiration of this work is based on the necessity to detect traces of this compound in fruits, a simple, low-cost, and sensitive SERS-active substrate built with silver nanoparticles (AgNPs) supported on a Si/ZnO nanowires platform was used. Aqueous dilutions of imazalil in trace concentrations were measured. Differences between SERS and normal Raman spectra, due to specific surface selection rules,[17,18] allowed us to propose the preferred orientation of the adsorbed molecule on the substrate surface. The comparison between the SERS spectral profiles of diluted samples of the pure compound and of the agricultural commercial product is significantly important if the presence of imazalil is sought to be detected in fruits using this analytical method.

2 | MATERIALS AND METHODS

Pure imazalil PESTANAL (analytical grade, Sigma-Aldrich) was used in solid state for the Fourier-transform infrared spectroscopy (FTIR) and normal Raman spectral acquisition. The agricultural commercial product imazalil Fecundal 50 EC (50% p/v, emulsifiable concentrate) was donated by the citrus company Citrícola San Miguel S. A., Argentina, and it was used without further purification to maintain the whole physical and chemical properties of the compound as normally used in fruit protection. A 10-μl drop of the commercial product was used for the acquisition of the FTIR and normal Raman spectra. For SERS measurements, different concentration stock solutions of the agricultural commercial product in the 10^{-5} M (3 ppm, approximately) to 10^{-7} M (0,03 ppm, approximately) range were prepared with distilled water. The SERS spectrum of a 10^{-5} M aqueous solution of pure imazalil was also acquired.

2.1 | Instrumentation

The FTIR spectra were acquired from pure imazalil compound contained in KBr pellets and from a film formed by a drop of the agricultural commercial product supported between KRS-5 windows. A FTIR Atti Mattson Genesis Series spectrometer was used. In order to improve the signal/noise ratio, 60 and 32 spectra in the 4,000–400 cm^{-1} range (4-cm^{-1} spectral resolution) were collected for the emulsifiable concentrate and the solid samples, respectively.

A DXR Raman microscope (Thermo Fisher Scientific) was used for normal Raman and SERS measurements. Normal Raman spectra between 3,500 and 50 cm^{-1} were acquired from 10-μl drops of the agricultural commercial product and from the solid sample of the pure imazalil. The samples in both states were deposited on gold-coated glass slides. Due to the strong fluorescence emission produced by the impurities contained in the commercial emulsifiable concentrate, the normal Raman spectrum of this sample was obtained by using a 780-nm excitation wavelength at 24 mW of power (5-cm^{-1} spectral resolution), instead of the 532-nm excitation (10 mW of power) used for the imazalil compound in pure state. Samples were focused with a 10× objective, and a 50-μm slit aperture was used for spectral collection. Spectra were obtained from six different sampling points and each spectrum resulted from accumulating 20 exposisions with an exposure time of 2 s each. For SERS measurements, Si/ZnO/AgNP substrates were used. Aqueous solutions of 10-μl volume at different concentrations were dropped onto the substrates and then naturally dried at room temperature. SERS measurements were acquired from three randomly selected locations within each substrate and the average spectrum calculated to minimize heterogeneities in the metal deposition. A 532-nm excitation wavelength (10-mW power) was used. Each spectrum was obtained by accumulating 40 exposisions of 2 s each. All measurements were performed at ambient temperature.

2.2 | Si/ZnO/AgNPs substrates

Substrates for SERS measurements were prepared following a protocol optimized in our laboratory, which will be published elsewhere with the corresponding characterization. Briefly, the first step consists of seeding ZnO onto undoped (111) oriented Si single crystal wafers, which were ultrasonically washed first with acetone, then in ethanol, and finally, distilled water. A 20-μl volume of zinc acetate dihydrate (proanalysis, Cicarelli) in ethanol 0.006 M was dropped on the wafers and distributed by spin coating at 1,000 RPM for 10 s. After rinsing with ethanol, the wafers were incubated at 330 °C for 30 min to yield ZnO seeds onto the silicon substrate. In the second step, ZnO nanowires were grown by a hydrothermal method.[19,20] Si wafers with ZnO seeds were immersed in an open crystallizing dish filled with an aqueous solution of zinc nitrate hydrate (0.025 M; proanalysis, Annedra) and hydroxymethylamine (0.025 M; pro-analysis, Merk) and subsequently incubated at 90 °C for 3 hr. Finally, AgNPs were deposited onto ZnO nanowires. This step was performed by immersing Si/ZnO substrates in a 0.1 M AgNO$_3$ solution prepared with a 1:1 ratio ethanol–water solution and subjecting them to UV-irradiation with 254-nm excitation for 12 min. These conditions would be suitable to produce plasmonic resonance on the AgNPs with the 532-nm laser because the substrates thus obtained have demonstrated to be SERS-active with a 10^{-7} M probe solution of crystal violet (data not shown here).

2.3 | Computational details

Quantum chemical calculations were performed with the Gaussian(R) 03 Program Package.[21] The grown state geometry of imazalil was fully optimized by using the density functional theory with the B3LYP hybrid functional[22–24] and the standard split valence basis set 6–311 + g(2df,p). Previously, rigid potential energy surface scans were performed at the B3LYP/6-31 g(d) level of theory to estimate the starting molecular geometry for optimization. Calculations were also performed for the imazalil molecule attached to a single silver atom (imazalil-Ag complex). The *gen* keyword was used, where the light atoms (CHNOCl) were calculated with the 6–311 + g(2df,p) basis set and the Ag atoms with the LANL2DZ basis set considering a pseudo potential. In order to determine the more probable orientations of imazalil on the silver surface, different locations of the Ag atom in the molecule vicinity were probed by evaluating the energies of the optimized complexes. The subsequent vibrational calculations, performed at the same level of theory than the optimizations, allowed

to ensure that the structures were true minima (imaginary wavenumbers were not obtained) and to determine the corresponding zero-point vibrational energies (ZPVEs). The calculated vibrational frequencies were scaled by an appropriated factor (0.9723) to match better with the experimental data. The vibration modes were identified and assigned with the aid of GaussView 5.0 graphical interface[25] that allows an interpretation of the predicted normal modes based on the atomic Cartesian displacements, reinforced by the corresponding displacement vectors.

3 | RESULTS AND DISCUSSION

3.1 | Conformational analysis and structural characterization of imazalil

The evaluation of the most stable conformation adopted by the imazalil molecule was performed by exploring the potential energy surface as a function of three dihedral angles that were separately varied. The preferred orientations of the aromatic rings and the vinyl group, with respect to the chiral C1 atom, were predicted with the B3LYP/6–31 g(d) method. Figure 1 shows the single-point energy calculations done for different values of the dihedral angles ϕ(C11–N4–C2–C1), ϕ(C10–C3–C1–C2), and ϕ(C22–C13–O7–C1) that determine the orientation of the imidazole, benzene, and vinyl groups, respectively. As was expected, flexibility around the C1–C3 bond is highly restricted due to steric interactions of the chlorine atom in *ortho* position with both CH$_2$ groups of the molecule. The most stable conformation is reached for the ϕ(C10–C3–C1–C2) = −90°. A second local minimum is calculated at ϕ = − 120° with an energy of 2.50 kcal.mol^{-1} above the global minimum. Similarly, the vinyl group appears also confined in a spatial region that keeps it apart from interactions with the π-electrons systems of both aromatic rings. In this scan, the zero energy value corresponds to a minimum occurring at ϕ(C22–C13–O7–C1) = 180°, which is centered in a wide trough with higher energies by 1.3, 0.45, and 1.85 kcal.mol^{-1} calculated for ϕ values of 150°, 210°, and 240°, respectively. In turn, the orientation of the imidazole-ring plane shows two minima at ϕ(C11–N4–C2–C1) = ±90°, and with an energy difference between them of only 0.27 kcal.mol^{-1}. In this case, the second minimum is separated from the first by an internal energy barrier of 4.31 kcal.mol^{-1}.

Figure 2 shows the fully optimized molecular geometry of the most stable conformer, as derived from the three global minima obtained. In the preferred arrangement, both aromatic rings planes are parallel to each other, whereas the allyl group attached to the O atom adopts such orientation that any steric and/or electronic
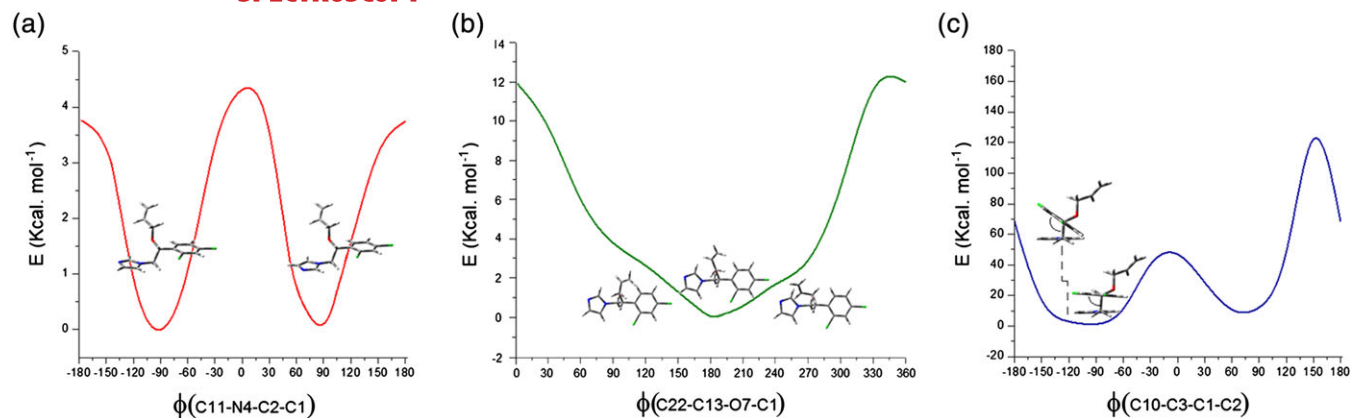
(a)

(b)

(c)

FIGURE 1 Rigid potential energy surface scans were performed at the B3LYP/6–31 g(d) level of theory. Three different coordinates were modified independently. In (a) and (c), the dihedral angles ϕ(C11–N4–C2–C1) and ϕ(C10–C3–C1–C2), respectively, were varied from −180° to 180°. In (b), the dihedral angle ϕ(C22–C13–O7–C1) was varied from 0° to 360°. The step size for each variable was 30°. For atom numbering see Figure 2 [Colour figure can be viewed at wileyonlinelibrary.com]
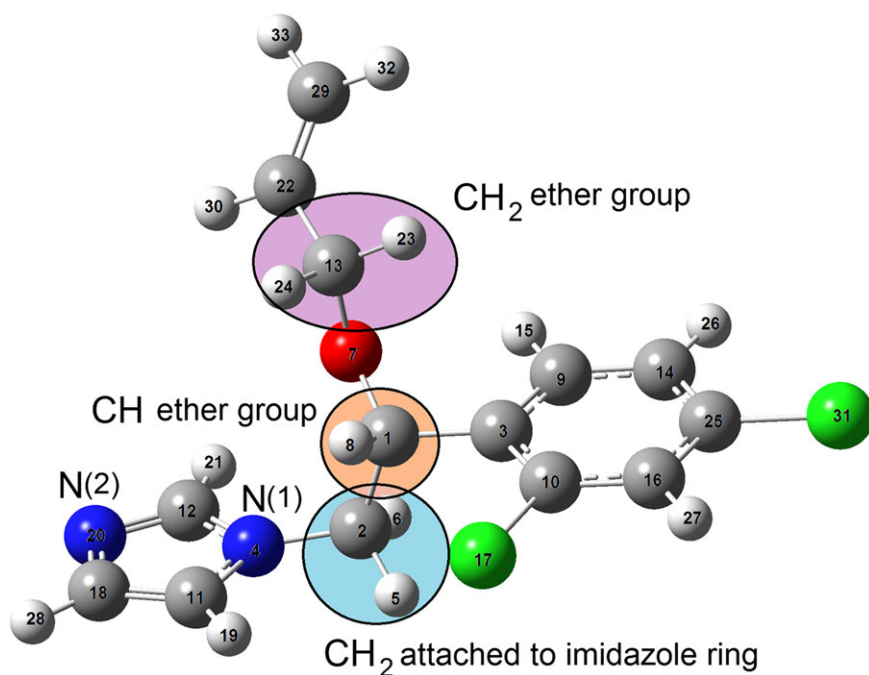

FIGURE 2 Optimized molecular structure of imazalil at the B3lyp/6–311 + g(2df,p) level of theory. Nitrogen atoms are renumbered as N(1) and N(2) and the methylene and methine groups with Csp^3 are marked and renamed as CH$_2$ *ether*, CH *ether*, and CH$_2$ attached *imidazole ring* as they are referred in the assignment tables [Colour figure can be viewed at wileyonlinelibrary.com]

interaction with the π electrons of the imidazol or benzene rings is minimized. The geometrical parameters, calculated with the B3LYP/6–311 + g(2df,p) method, are presented in Table 1.

3.2 | Vibrational characterization of imazalil

The experimental FTIR and normal Raman spectra in the 3,200–500 and 3,200–200 cm^{-1} ranges, respectively, of imazalil as pure substance and as the commercial concentrate pesticide, are shown in Figure 3. Calculated IR and Raman spectra for the isolated imazalil molecule,

performed with the B3LYP/6–311 + g(2df,p) method, are also included in Figure 3.

According to published vibrational analysis for related molecular systems, most of the bands appearing between 1,700 and 1,450 cm^{-1} are due to C=C and C=N stretchings of the vinyl group and the imidazole and benzene rings; several CH$_2$ deformations and in-plane-ring vibration modes of C$_{sp2}$-H, CCC, and CNC atomic groups are observed between 1,460 and 1,100 cm^{-1}, and the bands below 1,000 cm^{-1} are associated mainly with torsions and out-of-plane ring deformations; complex vibrations involving the C–O and C–Cl bonds appear in the 1,100–1,000 cm^{-1} range. A more detailed band

TABLE 1 The optimized geometrical parameters of imazalil, calculated at the B3LYP/6311 + g(2df,p) level of theory

Bond length (Å)		Bond angle (°)		Dihedral angle (°)	
C1–C2	1.538	C1C3C10	122.86	C1C3C10C16	178.81
C1–C3	1.522	C2C1C3	110.44	C2C1C3C10	−85.21
C1–O7	1.412	N4C2C1	113.15	N4C2C1C3	171.37
C2–N4	1.449	C9C3C10	117.01	C9C3C10C16	0.35
N4–C11	1.380	C11N4C2	126.52	C11N4C2C1	−84.50
N4–C12	1.364	C12N4C2	127.02	C12N4C2C1	91.40
C11–C18	1.367	C14C9C3	122.02	C14C9C3C10	−0.20
C18–N20	1.374	C18C11N4	105.74	C18C11N4C2	176.92
N20–C12	1.311	N20C12N4	112.19	N20C12N4C2	−177.00
C3–C9	1.395	O7C1C3	112.23	O7C1C3C10	155.74
C3–C10	1.395	C13O7C1	114.78	C13O7C1C3	−82.36
C9–C14	1.387	C22C13O7	108.64	C22C13O7C1	−174.42
C14–C25	1.388	C29C22C13	124.11	C29C22C13O7	−126.94
C25–C16	1.386	C25C16C10	118.74	C25C16C10C3	−0.26
C10–C16	1.389	Cl17C10C16	117.21	Cl17C10C16C25	179.63
C10–Cl17	1.756	Cl31C25C16	119.21	Cl31C25C16C10	179.92
C25–Cl31	1.745				
O7–C13	1.429				
C13–C22	1.494				
C22–C29	1.326				

assignment of the experimentally observed features was achieved based on the theoretical prediction of the vibrational behavior of the imazalil molecule. Only the most representative bands are discussed here, but the complete vibrational assignment for most of the FTIR and Raman bands is presented in Table 2.

The νC=C mode of the vinyl group is assigned to the intense band observed at 1,641 cm^{-1} in the Raman spectrum of the pure substance (1,635 cm^{-1}, weak feature in FTIR), in agreement with reported data for vinyl group in ethers and olefins.[26–28] The νC=C vibrations of substituted benzene rings are well characterized in bibliography.[27,29–31] Thus, the Raman bands observed at 1,590, 1,561 and 1,459 cm^{-1} are straightforward assigned to typical stretching modes of the benzene ring, showing good concordance with the theoretical predictions as well with the features observed in the spectra of the concentrate for agricultural uses. The intensity of the last band (1,459 cm^{-1}) in the Raman of the commercial pesticide suggests the presence of impurities/excipients contributing to the band shape. In this spectral region are also expected stretching vibrations localized in the imidazole ring: two medium-intensity Raman bands centered at 1,528 and 1,512 cm^{-1} have been published for methyl imidazole and at 1,535 and 1,488 cm^{-1} for imidazole in

neutral state, which have been briefly reported as ring vibrations,[32,33] and a medium-intensity band at 1,504 cm^{-1} has been observed in an N-substituted imidazole product and attributed to the stretching of the single C–N bond.[34] According to our calculations for the imazalil molecule, these vibrations can be characterized as the out-of-phase stretching of the C=C and C=N$_{(2)}$ bonds ($\nu_{o.o.ph}$ C=C/C=N$_{(2)}$) and the symmetric stretching ν_s CN$_{(1)}$C, which are predicted at 1,496 and 1,484 cm^{-1} and would be observed as the intense FTIR features at 1,502 and 1,469 cm^{-1}, respectively. This last band, not observed in the Raman spectra of imazalil, could be also attributed to a deformation mode of the CH$_2$ ether group, calculated at 1,464 cm^{-1} (see Table 2).

Two strong Raman bands centered at 1,363 and 1,346 cm^{-1} are observed in the spectrum of the pure substance, whereas in the commercial concentrate, a single intense albeit asymmetric band is observed; their FTIR counterparts are manifested as weak signals. According to the theoretical predictions, these features are associated to CH$_2$ and COC deformations as well as to the $\nu_{i.ph}$ C=C/C=N$_{(2)}$ mode.

In general, the νC–Cl modes in molecules with the halogen attached directly to a benzene ring are strongly coupled with different δCCC and δCH rings
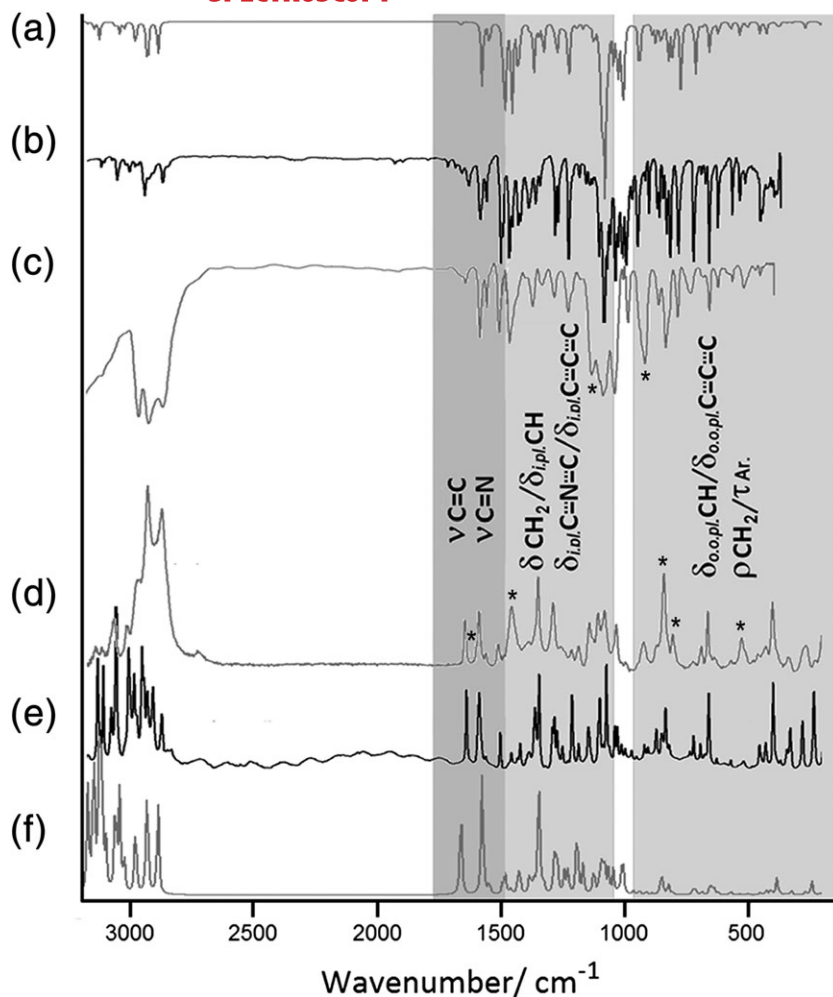
FIGURE 3 Experimental and calculated IR and Raman spectra for imazalil. (a,f) Theoretical IR and Raman spectra, respectively, predicted with the (B3LYP/6–311 + g (2df,p)) method. (b) FTIR spectrum of the pure imazalil supported in a KBr pellet. (c) FTIR spectrum of the agricultural commercial product acquired from a film supported between KRS-5 windows. (d) Raman spectrum of a 10-μl drop of the agricultural commercial product deposited on a gold glass slide. (e) Raman spectrum of the pure substance, obtained directly from the solid deposited on a gold glass slide. The commercial product was used without purification. All spectra were acquired at ambient temperature. *Bands showing high contributions from the impurities and/or excipients in the emulsifiable concentrate. Ar. = aromatic ring.

vibrations.[30,31] Our calculations predict additional couplings between the modes involving the halogen atoms with the asymmetric C–O–C stretching and other C–C vibrations, making a difficult unequivocal assignment. Thus, based on reported values for different chlorine-substituted benzene rings, the strongest FTIR bands at 1,087, 1,072, 1,041, and 1,030 cm^{-1} are tentatively associated with complex vibrations involving the C–Cl stretchings with the ν_{as} C–O–C, ρCH$_2$, and one $\delta_{i.pl.}$CCC modes. In the Raman spectrum of the pure imazalil, these fundamentals are observed as a very strong band at 1,074 cm^{-1} and two medium intensity bands at 1,041 and 1,030 cm^{-1}.

Most of the C–H and CCC out-of-plane deformations of both aromatic rings are predicted as mixed vibrations, appearing bellow 900 cm^{-1}. A tentative assignment of the experimental bands to these modes is proposed (Table 2).

The overall good correlation existing between the calculated wavenumbers and the bands observed in the spectra of the pure substance facilitates the identification of bands that could receive contributions from vibrational modes belonging to the impurities and/or excipients

present in the emulsifiable product. This is the case for the bands observed at 1,459, 840, 804, and 524 cm^{-1} in the Raman spectrum of this commercial sample, whose intensities differ considerably from the corresponding bands in the spectrum of the pure imazalil. The same interpretation is proposed for the intense bands observed at 1,138 and 922 cm^{-1} in the FTIR spectrum of the commercial agricultural product.

3.3 | SERS spectra of imazalil on Si/ZnO/AgNP substrate

The SERS spectrum of ~10^{-5} M aqueous solution of imazalil was measured. The spectral range between 1,700 and 500 cm^{-1} is presented in Figure 4. For comparison, the normal Raman spectrum of the pure imazalil and that of the clean substrate are included in the figure; also, a SEM image of the substrate is presented.

The Raman of the Si/ZnO/AgNP substrate shows a very strong and sharp band at 521 cm^{-1}, which is characteristic of the crystalline silicon, and a weak and flat band spanning from 940 to 980 cm^{-1}, typical of the SiO as thin film.[35] The SiO film is probably formed on the crystalline

TABLE 2 Calculated and experimental wavenumbers together with a tentative assignment for imazalil as pure substance and as emulsifiable concentrate pesticide

Imazalil (pure)		B3LYP/6–311 + g(2df,p)[b] (cm⁻¹)	Emulsifiable concentrate		Assignment[c]
Raman[a] (cm⁻¹)	FTIR[a] (cm⁻¹)		Raman[a] (cm⁻¹)	FTIR[a] (cm⁻¹)	
3,172 (vw)		3,171, 3,152			
3,135 (s)		3,144	3,147 (w)	3,149 (vw)	νC–H *imidazole ring*
3,124 (w)	3,124 (vw)	3,123	3,121 (w)	3,111 (w)	ν_{as} = CH_2 *vinyl group*
3,114 (s)	3,112 (vw)	3,114		3,084 (w)	νC–H *benzene ring*
3,080 (m)	3,080 (vw)	3,098			
3,061 (vs)	3,059 (m)	3,059 3,043	3,071 (m)		νC–H *vinyl group* ν_s=CH_2 *vinyl group*
3,010 (s)	3,009 (m)	3,024	3,016 (m)	ν_{as} CH_2 attach. *imidazole ring*	
2,988 (s) 2,955 (s)	2,988 (w) 2,947 (m)	2,978 2,933	2,970 (s, br)	2,968 (s)	ν_s CH_2 attach. *imidazole ring* ν_{as} CH_2 *ether* +C–H *ether*
2,934 (m)	2,933 (w)	2,929	2,934 (vs)	2,928 (s)	ν_{as} CH_2 *ether*−C–H *ether*
2,875 (m)	2,875 (m)	2,888	2,877 (vs)	2,871 (s)	ν_s CH_2 *ether*
1,641 (s)	1,635 (w)	1,664	1,646 (s)	1,647 (w)	νC=C *vinyl group*
			~1,600 (sh)[d]		
1,590 (s)	1,589 (s)	1,578	1,589 (s)	1,589 (s)	νC=C *benzene ring*
1,561 (w)	1,561 (m)	1,549	1,561 (m)	1,561 (w)	νC=C *benzene ring*
1,504 (m)	1,502 (s)	1,496 1,484	1,511 (m)	1,511 (s)	$\nu_{o.o.ph.}$ C=C/C=$N_{(2)}$ *imidazole ring* ν_s C$N_{(1)}$C *imidazole ring*
1,459 (w) 1,435 (w)	1,469 (s) 1,459 (m) 1,434 (m)	1,464 1,457 1,433	1,459 (s,br)[d]	1,469 (s) 1,460 (sh) 1,440 (sh)	δ CH_2 *ether* νC=C *benzene ring* δ CH_2 *imidazole ring*
1,423 (m)	1,423 (m)	1,426	1,426 (sh)		δ CH_2 *vinyl group*
1,387 (w)	1,391 (m)	1,386 1,371	1,387 (w,br)	1,375 (m)	δ CH ν_{as} C$N_{(1)}$C *imidazole ring*
1,363 (s) 1,346 (s) 1,320 (vvw)	1,363 (m) 1,346 (w)	1,367 1,350 1,346 1,329	1,349 (s)	1,346 (sh) 1,338 (w)	δ CH_2 + δ COC Wag. CH_2 attach. *imidazole ring* $\nu_{i.ph.}$ C=C/C=$N_{(2)}$ *imidazole ring* δ CH_2 attach. *imidazole ring*
1,293 (m) 1,285 (m) 1,274 (m)	1,285 (m) 1,274 (m)	1,289 1,283 1,276	1,289 (s)	1,289 (m)	δ CH δ CH *vinyl group* $\delta_{i.pl.}$ CH *imidazole ring* + $\delta_{i.pl.}$C$N_{(1)}$C
1,252 (m) 1,233 (vw)	1,230 (s)	1,255 1,245 1,233	1,257 (w,br)		$\delta_{i.pl.}$ CCC *benzene ring* $\delta_{i.pl.}$ CH *benzene ring* τ CH_2
1,216 (s)	~1,214 (sh)	1,228		1,232 (m)	$\delta_{i.pl.}$ CH *imidazole ring*
1,186 (m)	1,186 (w)	1,195	1,184 (m)	1,184 (w)	τ CH_2 *imidazole ring* + ν C_{sp3}-C_{sp2} *benzene ring*
1,147 (m)	1,144 (vw)	1,170	1,141 (s)	1,138 (vs)[d]	ν C_{sp3}–C_{sp2} *benzene ring* + $\delta_{i.pl.}$ CH *benzene ring*
1,107 (m)	1,10 7(s)	1,104	1,106 (s)	1,106 (vs)	$\delta_{i.pl.}$ CH *imidazole ring* + $\delta_{i.pl.}$C$N_{(2)}$C
1,087 (w)	1,087 (vs)	1,093		1,092 (vs)	ν_{as} C–O–C + $\nu_{i.ph.}$ C–Cl
1,074 (vs)	1,072 (m)	1,082	1,080 (s)	1,080 (sh)	ν_{as} C–O–C + $\nu_{i.ph.}$ C–Cl

TABLE 2 (Continued)

Imazalil (pure)		B3LYP/6–311	Emulsifiable concentrate		
Raman[a] (cm^{-1})	FTIR[a] (cm^{-1})	+ g(2df,p)[b] (cm^{-1})	Raman[a] (cm^{-1})	FTIR[a] (cm^{-1})	Assignment[c]
1,062 (w)	1,061 (m)	1,068	,		$\delta_{i.pl.}$ CH *imidazole ring*
1,041 (m)	1,041 (s)	1,048		1,046 (vs)	$\nu_{o.o.ph.}$ C–Cl + ρ CH$_2$ attach. *imidazole ring*
1,030 (m)	1,030 (m)	103	1,033 (s)		ν C–Cl + $\delta_{i.pl.}$ CCC *benzene ring*
1,013 (w)	1,013 (m)	1,015 1,008	1,010 (vw)	1,010 (w)	$\delta_{i.pl.}$ CN$_{(1)}$C *imidazole ring* ν_s C–O–C
998 (w)	997 (m)	1,005	995 (w)	992 (m)	$\delta_{o.o.pl.}$ CH *vinyl group*
955 (w)	952 (m)	943		947 (sh)	Wag=CH2 *vinyl group*
920 (w)	921 (vw)	915	922 (m)	922 (s)[d]	$\delta_{i.pl.}$ CH *vinyl group*
907 (w)	905 (w)	892			$\delta_{i.pl.}$ CN$_{(2)}$C *imidazole ring*
872 (m)	871 (w) 863 (w)	878 860	866 (m)	866 (m)	$\delta_{o.o.pl.}$ CH *benzene ring* ρ CH$_2$ attach. *imidazole ring* + ν C$_{sp3}$–C$_{sp3}$
850 (m) 835 (s)	847 (w) 834 (m)	853 848	840 (s)[d]	840 (s)	$\delta_{o.o.pl.}$ CH *imidazole ring* $\delta_{o.o.pl.}$ CH *benzene ring* + $\delta_{o.o.pl.}$ CH *imidazole ring*
820 (w)	818 (m)	825			$\delta_{o.o.pl.}$ CH *benzene ring*
		802	804 (m)[d]		$\delta_{o.o.pl.}$ CH *imidazole ring*
	787 (m)	775		790 (m)	ν C–Cl + δ C$_{sp2}$–C$_{sp3}$–C$_{sp3}$
724 (m)	724 (s)	724			$\delta_{o.o.pl.}$ CCC *benzene ring*
696 (m)	694 (w)	689	688 (m)	688 (w, sh)	$\delta_{i.pl.}$ CCC *benzene ring* + $\delta_{i.pl.}$ CNC *imidazole ring*
662 (vs)	662 (s)	659	660 (s)	660 (m)	τ *imidazole ring*
630 (w)	625 (m)	623	629 (w)	629 (w)	τ *imidazole ring*
523 (w)		507	524 (m)[d]	523 (m)	Skeletal
456 (m)	450 (m)	456			$\delta_{o.o.pl.}$ CCC *benzene ring*
433 (m)		431			$\delta_{o.o.pl.}$ CCC *benzene ring*
402 (vs)		388	398 (s)		$\delta_{o.o.pl.}$ CCC *benzene ring*
282 (vs)		272			Skeletal
238 (vs)		246	263 (m)		Wag. *imidazole ring*
193 (vs)		188	195 (s)		δ_s ClCC

[a]s, Strong; vs, very strong; m, medium; w, weak; vw, very weak; sh, shoulder; br, broad.

[b]All the wavenumbers were scaled by 0.9723.

[c]ν, Stretch; δ, deformation; ρ, rocking; τ, torsion; wag, wagging; s, symmetric; as, antisymmetric; i.pl., in-plane; o.o.pl., out-of-plane; i.ph., in-phase; o.o.ph., out-of-phase.

[d]Denotes bands that receive contributions from vibrations associated to impurities and/or excipients present in the commercial product for agriculture.

Si wafer by surface oxidation during the manufacturing process of the SERS-substrates.

The SERS spectrum of imazalil shows several bands that correlate well with the normal Raman spectrum of the pure substance. However, to support the interpretation of the observed bands, geometry optimizations and vibrational predictions of various imazalil-Ag complexes (B3LYP/6–311 + g(2df,p)/LANL2DZ) were performed. Figure 5 shows those imazalil-Ag complexes optimized at the lowest ZPVE values, which demonstrated to be true minima because no imaginary wavenumbers were obtained. By comparison among the corresponding energy values, it can be concluded that the imazalil molecule interacts with the metal through the
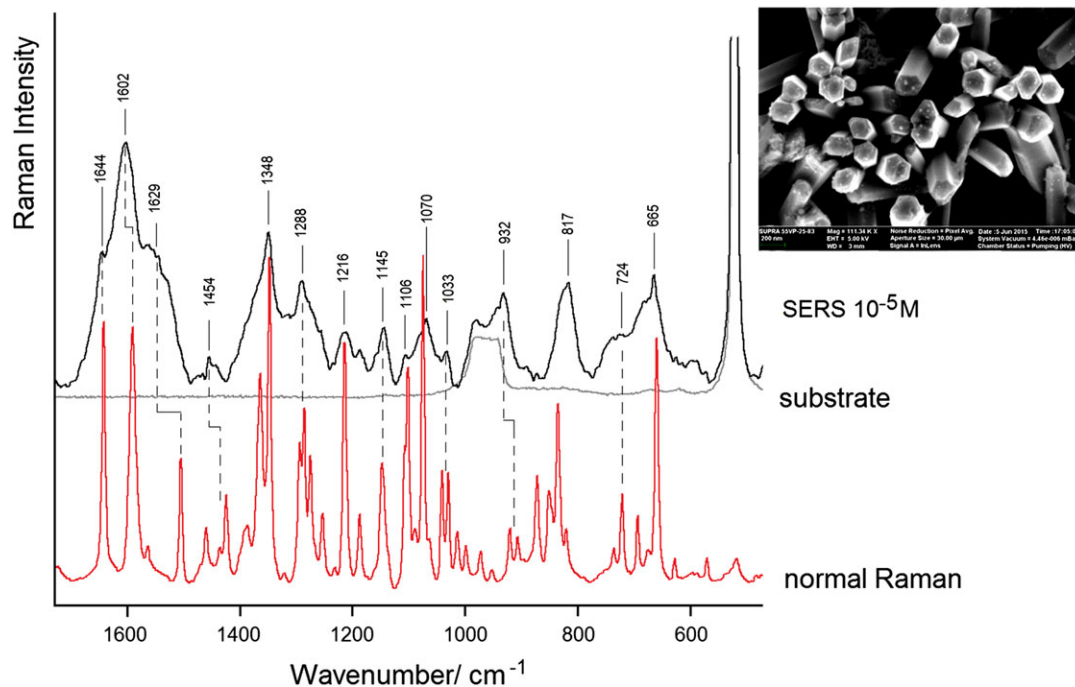
FIGURE 4 SERS spectrum between 1,700 and 500 cm^{-1} of a ~10^{-5} M aqueous solution of imazalil (black line). The normal Raman spectrum of imazalil as pure substance (red line) and the Raman spectrum of the Si/ZnO/AgNPs substrate (grey line) are included for comparison. In set: SEM image of the Si/ZnO/AgNPs substrate [Colour figure can be viewed at wileyonlinelibrary.com]
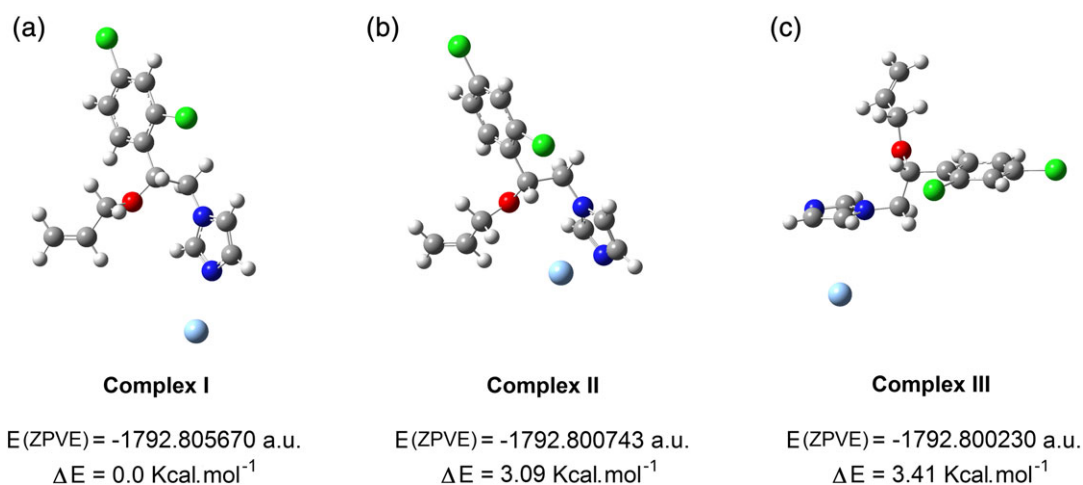

(a) Complex I
E(ZPVE) = -1792.805670 a.u.
ΔE = 0.0 Kcal.mol^{-1}

(b) Complex II
E(ZPVE) = -1792.800743 a.u.
ΔE = 3.09 Kcal.mol^{-1}

(c) Complex III
E(ZPVE) = -1792.800230 a.u.
ΔE = 3.41 Kcal.mol^{-1}

FIGURE 5 Optimized conformations of the three most stable imazalil-Ag complexes. Calculations were performed with the B3lyp/6–311 + g(2df,p) method for H, C, N, and O atoms and with the LANL2DZ basis set for Ag atom. Zero-point corrected energies (ZPVE) in Hartree and the energy differences (ΔE) in kcal.mol^{-1} with respect to the lowest ZPVE value are included [Colour figure can be viewed at wileyonlinelibrary.com]

imidazole ring moiety, whereas interactions through the π-electrons system of the benzene ring can be ruled out due to the significantly high energies (data not shown).

Previous studies of imidazole by SERS have shown that this molecule can adsorb onto a metal surface in two different ways: through the unshared pair of electrons on the N$_{(2)}$ atom or through the π-electrons system of the imidazole ring.[36] Coordination through the N$_{(2)}$ atom leads the molecule to adopt a perpendicular orientation of the aromatic ring plane with respect to the metal surface,[36] as was also observed for other heteroaromatic rings.[37–39] In the case of imazalil, this type of coordination implies that the vinyl group may also interact with

the metal through the π electrons of the C=C double bond. In effect, the imazalil-Ag complex showing the lowest ZPVE value is that with the metal interacting with the $N_{(2)}$ atom but, due to the proximity of the vinyl group, the optimization converged leaving the silver atom in a position slightly deviated from the coplanarity with the imidazole group (see Complex I in Figure 5). Other possible arrangements show the metal atom interacting with the

π-electrons system of the imidazole on both ring faces. Complexes II and III present $\Delta E = 3.09$ kcal.mol^{-1} and $\Delta E = 3.41$ kcal.mol^{-1} relative to Complex I, respectively.

Table 3 lists the SERS bands shown in Figure 4 together with the corresponding wavenumbers predicted for the most probable imazalil-Ag complex. According to the observed and calculated features, it is proposed that the band originated by the $\nu_{o.o.ph}C=C/C=N_{(2)}$ mode

TABLE 3 SERS bands observed in the 1,700–500 cm^{-1} spectral range of 10^{-5} M aqueous solutions of imazalil as pure substance and as commercial pesticide for agricultural uses

SERS pure Imazalil (cm^{-1})	SERS commercial pesticide (cm^{-1})	Complex I B3LYP/6–311 + g(2df,p)/LANL2DZ[a,b] (cm^{-1})	Assignment[c]
1,644		1,664	νC=C vinyl group
1,602	1,601	1,577	νC=C benzene ring/H$_2$O/impurity
1,564		1,548	νC=C benzene ring
1,547/1,529		1,501 (+5) 1,492 (+8)	$\nu_{o.o.ph.}$ C=C/C=N$_{(2)}$ imidazole ring ν_s CN$_{(1)}$C imidazole ring
1,454	1,450	1,466	νC=C benzene ring/impurity/excipient
1,348	1,352	1,346 (−4) 1,345	Wag. CH$_2$ attach. imidazole ring $\nu_{i.ph.}$ C=C/C=N$_{(2)}$ imidazole ring
1,288	1,300	1,288 1,282	δ CH δ CH vinyl group
1,270		1,277	$\delta_{i.pl.}$ CH imidazole ring + $\delta_{i.pl.}$CN$_{(1)}$C
1,256		1,254 1,245	$\delta_{i.pl.}$ CCC benzene ring $\delta_{i.pl.}$ CH benzene ring
1,216		1,229	$\delta_{i.pl.}$ CH imidazole ring
1,188		1,198	τ CH$_2$ imidazole ring + ν C$_{sp3}$–C$_{sp2}$ benzene ring
1,145	1,152	1,170	ν C$_{sp3}$–C$_{sp2}$ benzene ring + $\delta_{i.pl.}$ CH benzene ring
1,106		1,101 (−3)	$\delta_{i.pl.}$ CH imidazole ring + $\delta_{i.pl.}$CN$_{(2)}$C
1,070	1,063	1,081 1,073 (+5)	ν_{as} C–O–C + $\nu_{i.ph.}$ C–Cl $\delta_{i.pl.}$ CH imidazole ring
1,033	1,030	1,050 1,016	ρ CH$_2$ attach. imidazole ring $\delta_{i.pl.}$ CN$_{(1)}$C imidazole ring
	1,000		Impurity/excipient
932		915 904 (+12)	$\delta_{i.pl.}$ CH vinyl group $\delta_{i.pl.}$ CN$_{(2)}$C imidazole ring
	894		Impurity/excipient
	874		Impurity/excipient
817	822	849 817 (+15)	$\delta_{o.o.pl.}$ CH benzene ring / imidazole ring $\delta_{o.o.pl.}$ CH benzene ring
724		725	$\delta_{o.o.pl.}$ CCC benzene ring
674		688	$\delta_{i.pl.}$ CCC benzene ring + $\delta_{i.pl.}$ CNC imidazole ring
665		654	τ imidazole ring

[a]All the wavenumbers were scaled by 0.9723.

[b]Data in parentheses are the difference between calculated wavenumbers for Complex I and imazalil molecule.

[c]ν, Stretch; δ, deformation; ρ, rocking; τ, torsion; wag, wagging; s, symmetric; as, antisymmetric; i.pl., in-plane; o.o.pl., out-of-plane; i.ph., in-phase; o.o.ph., out-of-phase.

experiences an important upshift upon SERS effect (from 1,504 to 1,529 or 1,547 cm^{-1}), and the irregular band contour on the low wavenumber side indicates that the ν_s CN$_{(1)}$C mode becomes more active. These interpretations are in concordance with the expected interaction of the imazalil molecule with the metal surface: The corresponding wavenumbers for both vibrations in Complex I are predicted experiencing blueshifts. Similarly, the $\delta_{i.pl.}$ CN$_{(2)}$C mode (observed at 907 cm^{-1}in the normal Raman spectrum of the pure substance) can be associated with the SERS band at 932 cm^{-1}. The strong SERS band at 1,602 cm^{-1} could be assigned to the benzene νC=C mode (the strong band at 1,590 cm^{-1} in the normal Raman spectrum). However, interactions of the benzene ring with the metal are not predicted to justify a shift of this band. Alternatively, this intense band may be related to the presence of water molecules in interaction with the metal surface, according to reported SERS spectra of pure water that showed a band[39,40] at 1,610 cm^{-1}.

The presence of SERS bands corresponding to both the in-plane and out-of-plane vibration modes of the imidazole and benzene aromatic rings suggests that imidazol adopts a tilted orientation with respect to the metal surface.[41,42] However, the possibility that the molecule is also adsorbed on the metallic surface with a flat orientation of the imidazole ring is not ruled out.

3.4 | SERS spectra of the imazalil product for agricultural uses

Figure 6 compares the SERS spectra, in the region of 1,700 to 600 cm^{-1}, of the aqueous solutions of imazalil (10^{-5} M) as product for agricultural use and as pure substance. In general, the SERS spectral profile of the commercial pesticide evidences several bands that correlate well with those observed in the SERS spectrum of the pure imazalil, but exhibiting weaker intensities. The SERS bands of the commercial sample are included in Table 3.

In the spectrum of the commercial pesticide, the band centered at 1,450 cm^{-1} stands out. Due to its intensity and band shape, this feature is associated with vibrations corresponding to impurity and/or excipient present in the sample. The sharp band observed at 1,000 cm^{-1} as well as those at 894 and 874 cm^{-1} would also be attributable to the presence of impurities.
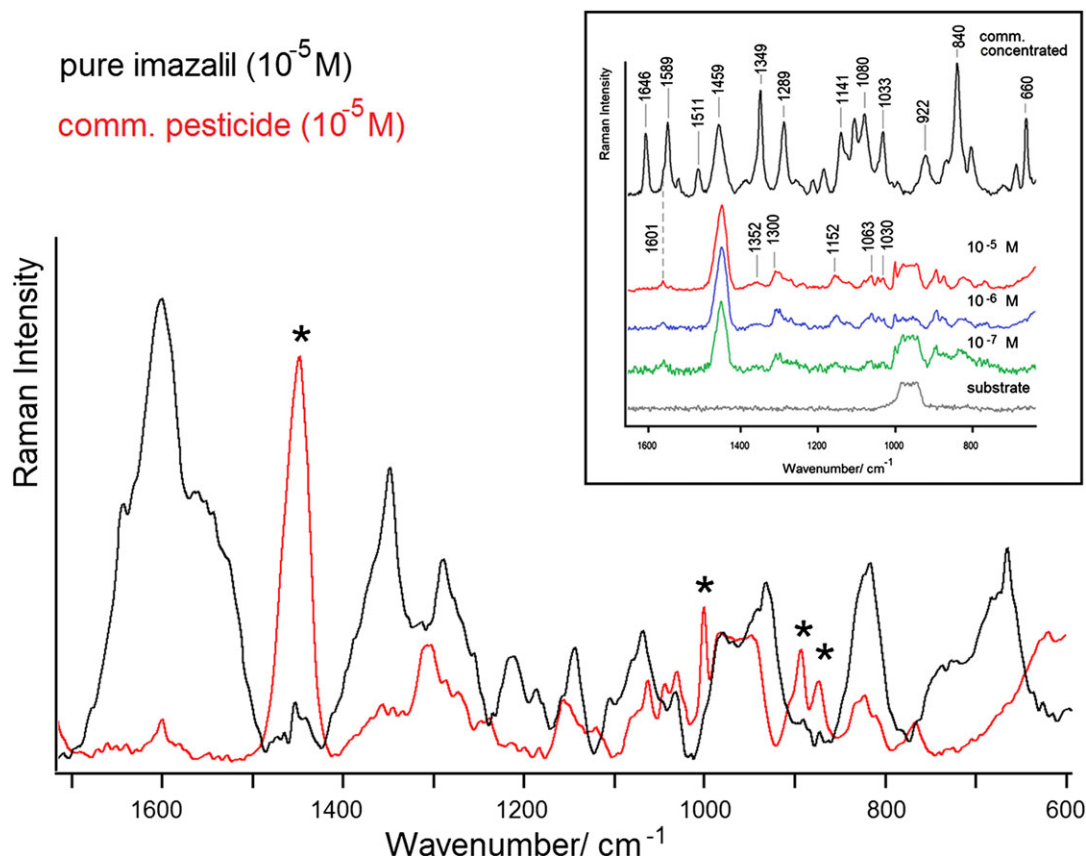

FIGURE 6 SERS spectra in the 1,700 and 600 cm^{-1} range of aqueous solutions of imazalil (10^{-5} M) as a pesticide for agricultural use (red line) and as a pure substance (black line). In set: Series of SERS spectra of aqueous solutions of the commercial pesticide at different concentrations: 10^{-5} M, 10^{-6} M, and 10^{-7} M, together with the normal Raman spectrum of imazalil as commercial concentrate and the Raman spectrum of the Si/ZNO/AgNPs substrate [Colour figure can be viewed at wileyonlinelibrary.com]

4 | CONCLUSIONS

The complete vibrational analysis of imazalil as pure substance in solid state and as a commercial pesticide product is presented here. Quantum chemical calculations allowed a reliable assignment of most of the observed IR and Raman bands. This study constitutes the starting point for the implementation of SERS as a trace detection method for imazalil as contaminant in fruits and foods.

Although the strongest band in the SERS spectra of the commercial agricultural product (1,450 cm^{-1}) is interpreted as receiving remarkable contributions from vibrations of impurities or excipients in the sample, the detection of other several features, albeit weak, offers a promising prospect for the use of the Si/ZnO/AgNPs-based substrates for determinations of the contaminant imazalil by SERS.

Interpretation of the SERS spectrum of the pure substance relies on computational predictions of the main binding sites of a silver atom to the different functional groups of the imazalil molecule. Correlation between the vibrational behavior predicted for the imazalil-Ag complex with the lowest ZPVE value with the experimentally observed features allowed proposing the most probable adsorption orientation. These results are important for subsequent uses of the novel Si/ZnO/AgNP-based substrate for fast, low-cost, and sensitive detection of this contaminant.

ORCID

Rosa M.S. Álvarez http://orcid.org/0000-0002-5468-0705

REFERENCES

[1] M. F. Franco-Bernardes, M. Pazin, L. C. Pereira, D. J. Dorta, *Toxicology Studies—Cells, Drugs Environment*, InTech, Croatia **2015** 195.

[2] C. C. Leandro, P. Hancock, R. J. Fussell, B. J. Keely, *J. Chromatogr. A* **2006**, *1103*, 94.

[3] J. Fillion, F. Sauvé, J. Selwyn, *J. AOAC Int.* **2000**, *83*, 698.

[4] S. R. Ananda Gowda, R. K. Somashekar, *Bull. Environ. Contam. Toxicol.* **2012**, *89*, 626.

[5] S. Grimalt, P. Dehouck, *J. Chromatogr. A* **2016**, *1433*, 1.

[6] S. Pang, T. Yang, L. He, *TrAC, Trends Anal. Chem.* **2016**, *85*, 73.

[7] L. Yande, Z. Yuxiang, W. Haiyang, Y. Bing, *Int. J. Agric. Biol. Eng.* **2016**, *9*, 179.

[8] A. Kim, S. J. Barcelo, Z. Li, *Nanotechnology* **2015**, *26*, 15502.

[9] B. Wang, L. Zhang, X. Zhou, *Spectrochim. Acta Part A Mol. Biomol. Spectrosc.* **2014**, *121*, 63.

[10] C. Müller, L. David, V. Chis, S. C. Cinta, *Food Chem.* **2014**, *145*, 814.

[11] J. C. S. Costa, R. A. Ando, A. Sant'Ana, P. Corio, *Phys. Chem. Chem. Phys.* **2012**, *14*, 15645.

[12] M. Fleischmann, P. Hendra, A. McQuillan, *Chem. Phys. Lett.* **1974**, *26*, 163.

[13] M. Moskovits, *Rev. Mod. Phys.* **1985**, *57*, 783.

[14] M. Fan, G. F. S. Andrade, A. G. Brolo, *Anal. Chim. Acta* **2011**, *693*, 7.

[15] D. Ortelli, E. Patrick, C. Corvi, *Food Addit. Contam.* **2005**, *22*, 423.

[16] M. R. Siegel, N. N. Ragsdale, *Pestic. Biochem. Physiol.* **1978**, *9*, 48.

[17] E. Le Ru, S. Meyer, C. Artur, P. Etchegoin, J. Grand, P. Lang, F. Maurel, *Chem. Commun.* **2011**, *47*, 3903.

[18] J. Cabalo, J. A. Guicheteau, S. Christesen, *J. Phys. Chem. A* **2013**, *117*, 9028.

[19] L. E. Greene, M. Law, D. H. Tan, M. Montano, J. Goldberger, G. Somorjai, P. Yang, *Nano Lett.* **2005**, *5*, 1231.

[20] L. E. Greene, B. D. Yuhas, M. Law, D. Zitoun, P. Yang, *Inorg. Chem.* **2006**, *45*, 7535.

[21] M. J. Frisch, G. W. Trucks, H. B. Schlegel, G. E. Scuseria, M. A. Robb, J. R. Cheeseman, J. A. Montgomery Jr., T. Vreven, K. N. Kudin, J. C. Burant, J. M. Millam, S. S. Iyengar, J. Tomasi, V. Barone, B. Mennucci, M. Cossi, G. Scalmani, N. Rega, G. A. Petersson, H. Nakatsuji, M. Hada, M. Ehara, K. Toyota, R. Fukuda, J. Hasegawa, M. Ishida, T. Nakajima, Y. Honda, O. Kitao, H. Nakai, M. Klene, X. Li, J. E. Knox, H. P. Hratchian, J. B. Cross, V. Bakken, C. Adamo, J. Jaramillo, R. Gomperts, R. E. Stratmann, O. Yazyev, A. J. Austin, R. Cammi, C. Pomelli, J. W. Ochterski, P. Y. Ayala, K. Morokuma, G. A. Voth, P. Salvador, J. J. Dannenberg, V. G. Zakrzewski, S. Dapprich, A. D. Daniels, M. C. Strain, O. Farkas, D. K. Malick, A. D. Rabuck, K. Raghavachari, J. B. Foresman, J. V. Ortiz, Q. Cui, A. G. Baboul, S. Clifford, J. Cioslowski, B. B. Stefanov, G. Liu, A. Liashenko, P. Piskorz, I. Komaromi, R. L. Martin, D. J. Fox, T. Keith, M. A. Al-Laham, C. Y. Peng, A. Nanayakkara, M. Challacombe, P. M. W. Gill, B. Johnson, W. Chen, M. W. Wong, C. Gonzalez, J. A. Pople, *Revision E.01*, *Gaussian*, Inc., Wallingford CT **2003**.

[22] C. Lee, W. Yang, R. G. Parr, *Phys. Rev. B* **1988**, 37.

[23] A. D. Becke, *J. Chem. Phys.* **1993**, 98.

[24] P. J. Stephens, F. J. Devlin, C. F. Chabalowski, M. J. Frisch, *J. Phys. Chem.* **1994**, *98*, 11623.

[25] R. Dennington II, T. Keith, J. Millam, K. Eppinnett, W. L. Hovell, R. Gilliland, *GaussView version 4.1*, Semichem, Shawnee Mission, KS, USA **2003**.

[26] H. Kimmel, W. H. Snyder, *Spectrosc. Lett.* **1971**, *4*, 15.

[27] N. B. Colthup, L. H. Daly, S. E. Wiberley, *Introduction to Infrared and Raman Spectroscopy*, 3rd ed., Academic Press, New York **1990**.

[28] D. W. Mayo, F. A. Miller, and R. W. Hannah, *Course Notes on the Interpretation of Infrared and Raman Spectra*, Wiley, New York **2004**, 73.

[29] R. M. S. Alvarez, R. N. Farías, P. Hildebrandt, *J. Raman Spectrosc.* **2004**, *35*, 947.

[30] X. Xuan, C. Zhai, *Spectrochim. Acta Part A Mol. Biomol. Spectrosc.* **2011**, *79*, 1663.

[31] M. Govindarajan, M. Karabacak, V. Udayakumar, S. Periandy, *Spectrochim. Acta Part A Mol. Biomol. Spectrosc.* **2012**, *88*, 37.

[32] D. A. Carter, J. E. Pemberton, *J. Raman Spectrosc.* **1997**, *28*, 939.

[33] J. Bukowska, A. Kudelski, K. Jackowska, *J. Electroanal. Chem.* **1991**, *309*, 251.

[34] V. Calvino-Casilda, M. A. Bañares, *Catal. Today* **2012**, *187*, 191.

[35] P. Borowicz, M. Latek, W. Rzodkiewicz, A. Łaszcz, *Adv. Nat. Sci. Nanosci. Nanotechnol.* **2012**, *7*, 45003.

[36] B. H. Loo, Y. Tse, K. Parsons, C. Adelman, Y. G. Lee, *J. Raman Spectrosc.* **2006**, *37*, 299.

[37] M. Muniz-Miranda, M. Pagliai, F. Muniz-Miranda, V. Schettino, *Chem. Commun.* **2011**, *47*, 3138.

[38] L. Chen, Y. Gao, H. Xu, Z. Wang, Z. Li, R. Zhang, *Phys. Chem. Chem. Phys.* **2014**, *16*, 20665.

[39] Y. Chen, A. Otto, *J. Raman Spectrosc.* **2005**, *36*, 736.

[40] J. Li, Y. Huang, S. Duan, R. Pang, D. Wu, B. Ren, X. Xu, Z. Tian, *Phys. Chem. Chem. Phys.* **2010**, *12*, 2493.

[41] A. Mühlig, D. Cialla-May, J. Popp, *J. Phys. Chem. C* **2017**, *121*, 2323.

[42] D. V. Chulhai, L. Jensen, *J. Phys. Chem. C* **2013**, *117*, 19622.